Cheerambathur et al. Figure S1

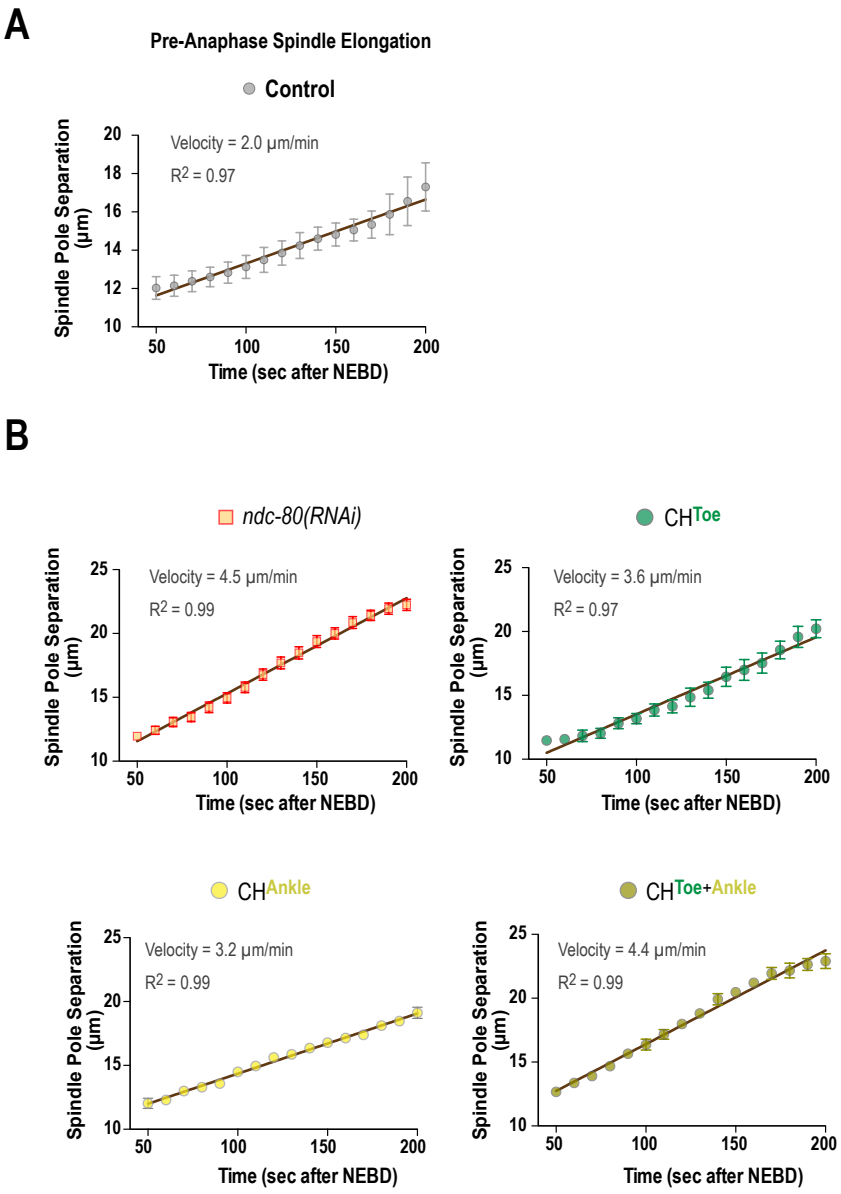

Figure S1 (Related to Figure 1). Pre-anaphase spindle pole separation rates in control and NDC-80 CH Domain mutants.

Linear regression fits were used to determine pole separation velocity for control (no RNAi) **(A)** and NDC-80 depletion as well as engineered CH domain mutants **(B)**. R squared values indicate the goodness of fit. The plotted data are the same as in *Fig. 1D*.

Cheerambathur et al. Figure S2

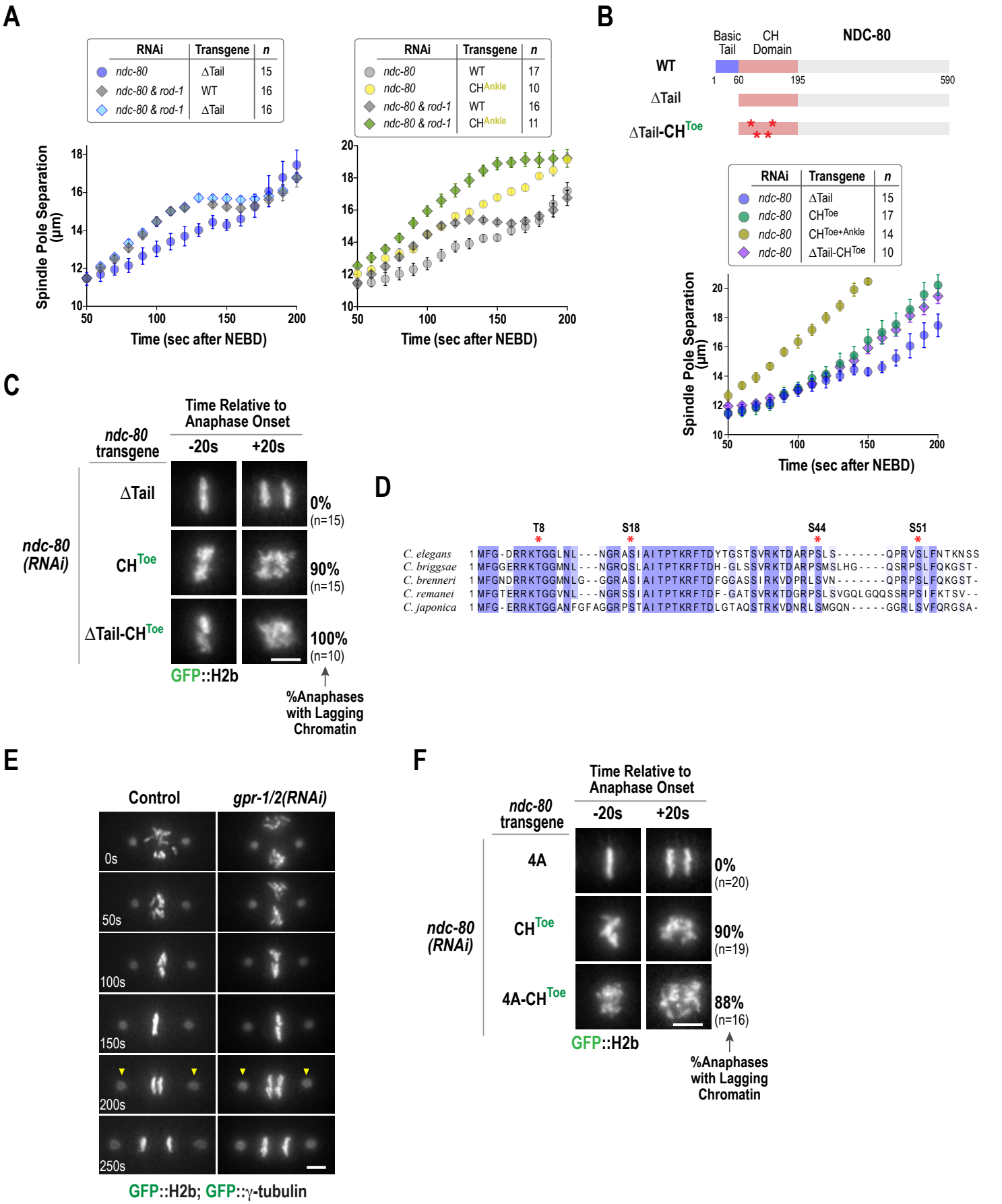

Figure S2 (Related to Figure 2). Phenotypic analysis of NDC-80 N-tail deletion, Gα pathway inhibition, and NDC-80 non-phosphorylatable 4A mutant.

(A) Spindle pole separation analysis of the indicated conditions. WT and CH^{Ankle} data are the same as in *Fig. 1B* & *1D*.

(B) Spindle pole separation analysis of the indicated conditions. CH^{toe} and $CH^{Toe + Ankle}$ data is the same as in *Fig. 1D* and ΔTail data is the same as in *Fig. 2A*.

(C) Chromosome segregation phenotypes for the indicated conditions highlighted by image stills from time-lapse movies 20 sec prior to and after anaphase onset. Numbers on right indicate percentage of one-cell embryo anaphases with detectable lagging chromatin. Scale bar, 5 μm.

(D) Sequence alignment of the NDC-80 N-tail from related nematode species. 4 conserved putative Aurora kinase phosphorylation sites are marked by asterisks.

(E) Stills from time-lapse sequences of control and Gα pathway-inhibited embryos in a strain co-expressing GFP::H2b and GFP-γ-tubulin. Scale bar, 5 μm.

(F) Chromosome segregation phenotypes for the indicated conditions highlighted by image stills from time-lapse movies 20 sec prior to and after anaphase onset. Numbers on right indicate percentage of one-cell embryo anaphases with detectable lagging chromatin. Scale bar, 5 μm.

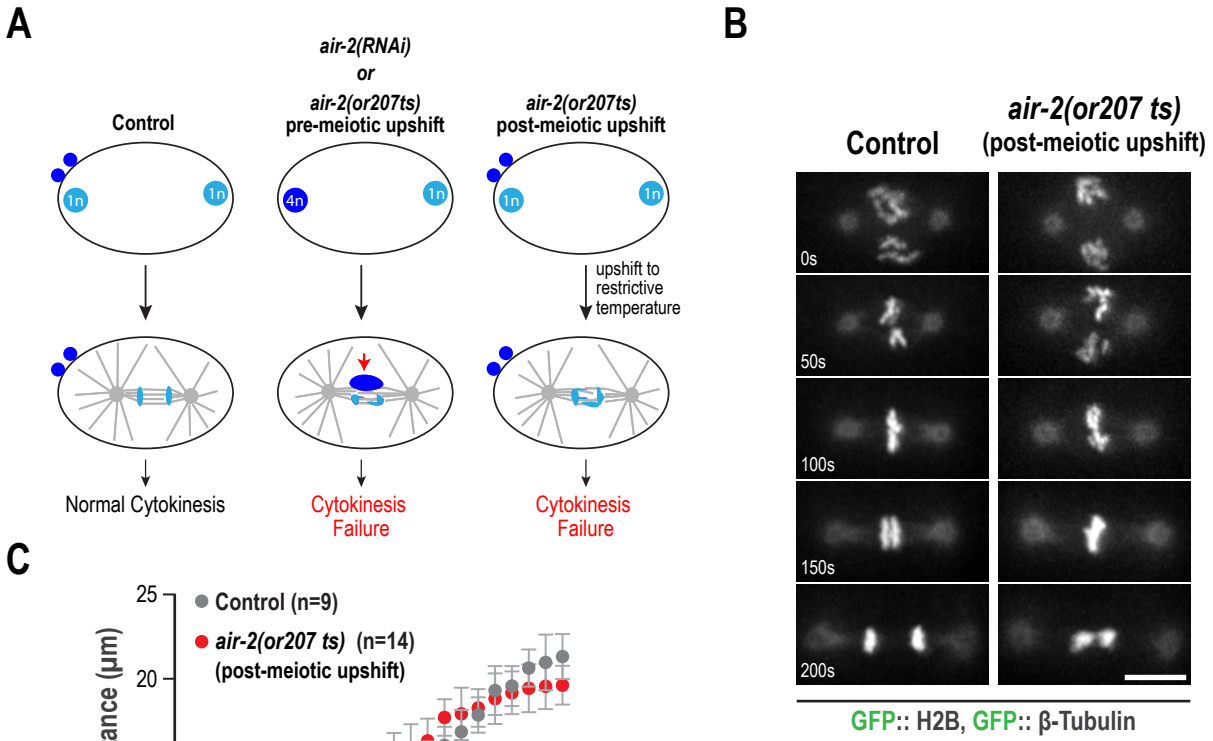
A
air-2(RNAi)
or
Control
air-2(or207ts)
pre-meiotic upshift
air-2(or207ts)
post-meiotic upshift
1n
4n
upshift to
restrictive
temperature
Normal Cytokinesis
Cytokinesis
Failure
Cytokinesis
Failure
B
Control
air-2(or207 ts)
(post-meiotic upshift)
0s
50s
100s
150s
200s
GFP:: H2B, GFP:: β-Tubulin
C
Control (n=9)
air-2(or207 ts) (n=14)
(post-meiotic upshift)
Pole-Pole Distance (µm)
Time from NEBD in sec
D
Control
tpxl-1(RNAi)
Time
(sec)
0
280
mCh::H2B; GFP::β-Tubulin
E
RNAi
n
None 6
tpxl-1 10
tpxl-1 + knl-1 8
tpxl-1 + ndc-80 10
Pole-Pole Distance (µm)
Time from NEBD in sec

Figure S3 (Related to Figure 2). Spindle pole separation analysis for a temperature-sensitive mutant of Aurora B/AIR-1 and depletion of the Aurora A/AIR-1 activator TPXL-1.

(A) Schematics describing phenotypes associated with Aurora B/AIR-2 inhibition in the one-cell *C. elegans* embryo. Following *air-2(RNAi)* or inactivation of the *air-2(or207ts)* mutant (Severson et al., 2000) prior to meiosis, oocyte meiotic segregation fails and the unsegregated maternal genome interferes with the zygotic division (*middle panels*). To avoid this mass of unsegregated DNA, the temperature up-shift in the *air-2(or207ts)* mutant is performed after meiosis is completed. Adapted from (Lewellyn et al., 2011) .

(B) Stills from time-lapse sequences depicting phenotype observed following Aurora B/AIR-2 inhibition employing the post-meiotic upshift protocol in the *air-2(or207ts)* mutant. All up-shifted mutant embryos exhibited segregation defects, premature decondensation of chromosomes, and failed cytokinesis. Scale bar 5 µm.

(C) Pole separation analysis of control and *air-2(or207ts)* mutant embryos imaged after post-meiotic upshift. Error bars are the 95% confidence interval. Inactivation of Aurora B by this approach does not result in the spindle pole separation phenotype observed with NDC-80^{4A}.

(D) Kymograph of the spindle region for a control embryo or following *tpxl-1(RNAi)* in a strain co-expressing mCh::H2b and GFP::β-tubulin. As shown previously, TPXL-1 depletion leads to spindle pole shortening after NEBD (Ozlü et al., 2005). The same phenotype is observed following selective mutation of TPXL-1 binding to Aurora A/AIR-1 ((Ozlü et al., 2005). Scale bar. 5 µm.

(E) Pole separation analysis for the indicated conditions. The effect of TPXL-1 depletion on pole separation is dependent on KNL-1 and on NDC-80. Kinetochore dynein depletion using *rod-1(RNAi)* does not affect the TPXL-1 phenotype (*not shown*). This result suggests that TPXL-1-activated

Aurora A/AIR-1 controls NDC-80-mediated attachments at kinetochores, as the effect of TPXL-1 depletion on pole separation is suppressed by NDC-80 depletion.

Cheerambathur et al. Figure S4

A

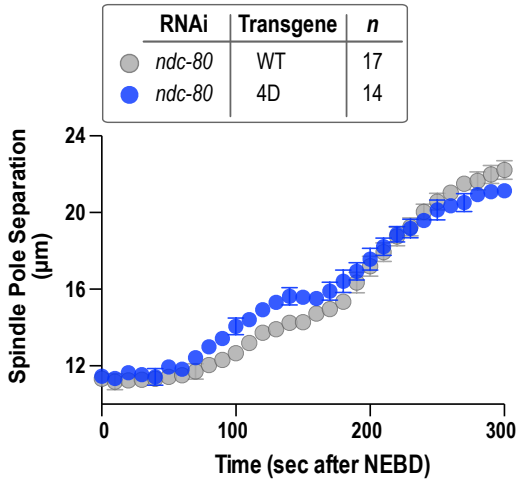

B

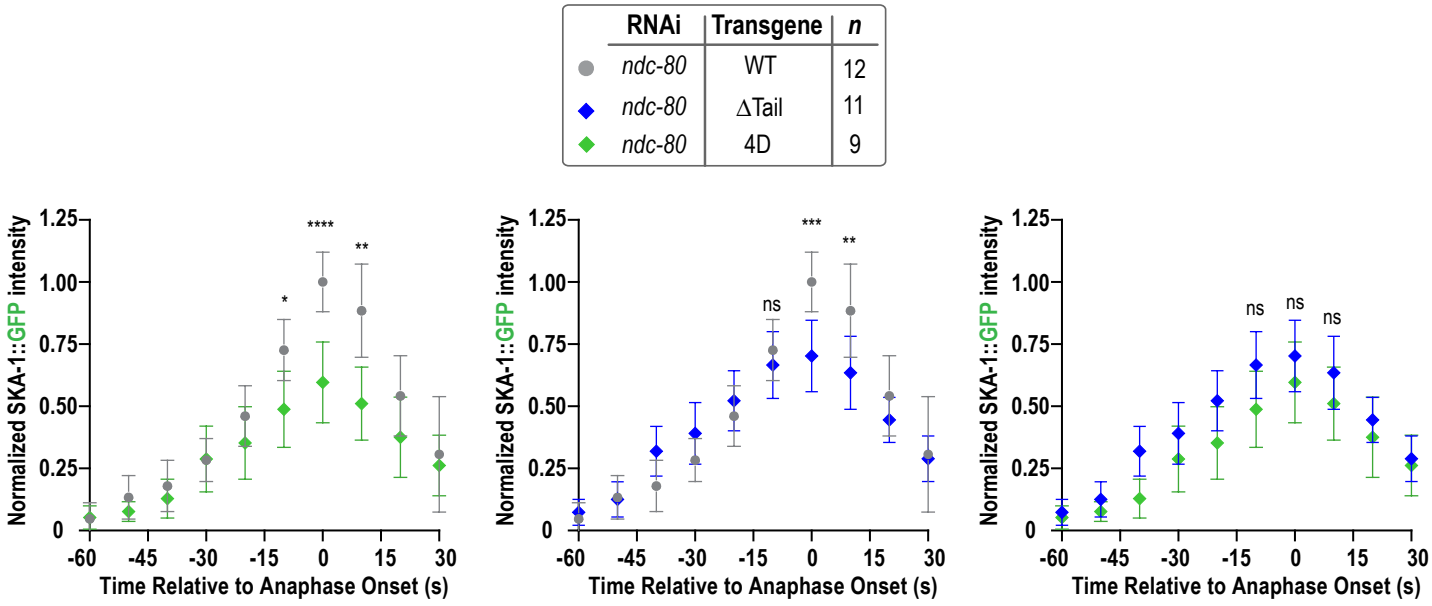

Figure S4 (Related to Figure 3). Spindle pole separation analysis for phosphomimetic NDC-80 and analysis of SKA-1::GFP chromosomal intensity.

(A) Spindle pole separation analysis of WT and phosphomimetic (4D) NDC-80. WT NDC-80 data is the same as in *Fig. 1B.*

(B) Analysis of SKA-1::GFP chromosomal intensity relative to anaphase onset for the indicated conditions. The data shown in *Fig. 3F* is re-plotted and *p*-values (****, ***, **, * and ns correspond to p-values of <0.001, 0.0001 to 0.001, 001 to 0.01, 0.01 to 0.05 and ≥0.05 respectively) calculated using unpaired *t*-tests in GraphPad Prism (GraphPad Software). Error bars are the 95% confidence interval.

Cheerambathur et al. Figure S5

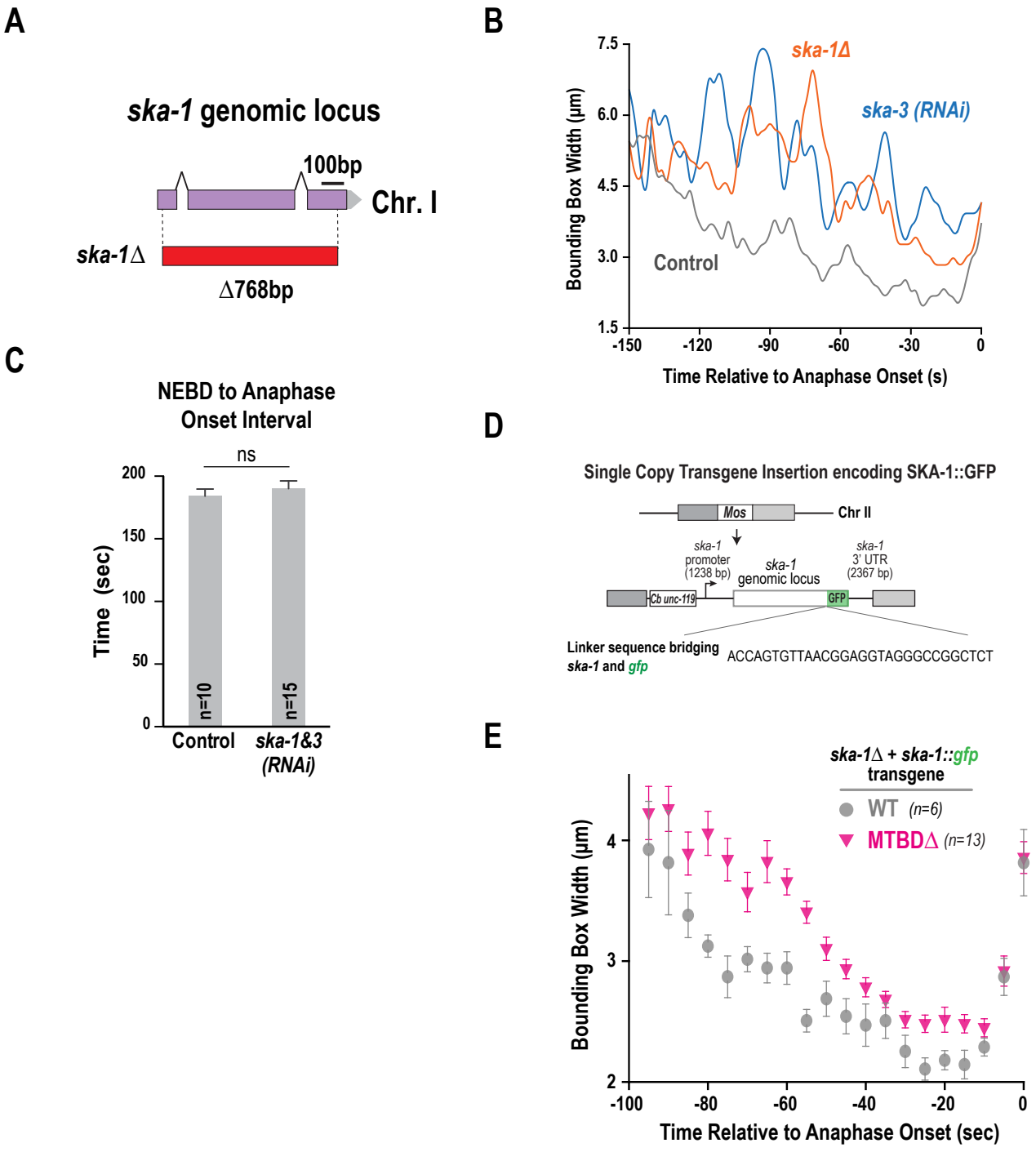

Figure S5 (Related to Figures 4 & 5). *ska-1Δ* and analysis of SKA complex inhibition.

(A) Schematic of the *ska-1* genomic locus and the *ska-1* deletion generated using CRISPR-Cas9. The deletion removes the majority of the *ska-1* coding region.

(B) Plots of the width of the bounding box that contains chromosomal fluorescence, measured as in *Fig. 4B*. Individual examples for control, *ska-1Δ* and *ska-3(RNAi)* are shown.

(C) Plot showing NEBD to anaphase onset interval in control and SKA-1/3 depleted embryos. There is no significant effect of SKA complex depletion on anaphase onset (p=0.14). Error bars are the S.D.

(D) Schematic of the SKA-1::GFP transgene targeted to a single Mos insertion on chromosome II.

(E) Average plot of chromosome distribution along the spindle axis for the indicated conditions. Error bars are the SEM.

Table S1: Oligonucleotides & templates used for dsRNA production (Related to Method Details in STAR Methods section)

Gene	Oligonucleotide 1	Oligonucleotide 2	Template
W01B6.9 (*ndc-80*)	5'- aattaaccctcactaaagg GATGACAAGTACATTCAGA GATTATACAAATGATC-3'	5'- taatacgactcactatagg GTGGTTCAAGATTCATTTGA ATATTAAGTCCACTG-3'	N2 cDNA
Y106G6H.15 (*ska-1*)	5'- aattaaccctcactaaagg TTATGGATAATAGAAAGTC AACG-3'	5'- taatacgactcactatagg ATGGAATCGTTTATTGATCG GAT-3'	N2 genomic DNA
F54E7.8 (*ska-3*)	5'- aattaaccctcactaaagg ATGGCTAACGAAACGCTG GAACATG-3'	5'- taatacgactcactatagg AACTCATCAAAAGCCAGTTT TCGTCG-3'	N2 genomic DNA
F22B7.13/ C38C10.4 (*gpr-1/2*)	5'- aattaaccctcactaaagg AGCATGTGATTCCACACGT CGC -3'	5'- taatacgactcactatagg TCTGGCAGCAGACAGTTCA GTTC -3'	N2 genomic DNA
Y43F4B.6 (*klp-19*)	5'- aattaaccctcactaaagg ATTGGGAGAGCTGGTGAA TG-3'	5'- taatacgactcactatagg GACTTTCCTACGTGCTTCGC-3'	N2 genomic DNA
Y39G10AR.12 (*tpxl-1*)	5'- aattaaccctcactaaagg GCGAACAAGGCAACAGCG CCG-3'	5'- taatacgactcactatagg TTTCTTCTCATACCCTTTGTA GGAGCT-3'	N2 genomic DNA

* Lowercase letters denote T3 and T7 sequences included for RNA synthesis.